CrossMark

Isotope-selective laser photoionization of tin in supersonic atomic beam

S. G. Nakhate[1,3] · Soumen Bhattacharyya[1,3] · Sheo Mukund[1] · Rita Behera[2,3] · Swarupananda Pradhan[2,3] ·
M. S. Bhatia[4] · V. M. Datar[4] · V. Nanal[4] · R. G. Pillay[4] · S. J. Wategaonkar[4]

Abstract

The isotope ^{124}Sn enriched to better than 50% is needed in substantial quantity as detector material for the proposed neutrinoless double beta decay (0νββ) experiment in India (*TIN.TIN*). Present work investigates isotope-selective laser photoionization scheme for ^{124}Sn. Transition to the first excited state from the ground state lies at 286.3 nm having short lifetime (~5 ns) and isotope shift (IS), $\Delta\nu(124–120) = 441$ MHz. However, the availability of high repetition rate (kHz), narrowband tunable pulsed laser in UV with low temporal jitter is a technological impediment for achieving isotopic selectivity in this transition. An alternate three-color photoionization scheme is proposed for separation of ^{124}Sn. Laser vaporization of tin followed by supersonic expansion in a molecular beam apparatus provided the tin atomic beam. Tin atoms were first excited to the $5p6s,^3P_1$ state from the $5p^2,^3P_0$ ground state by a broadband pulsed dye laser ($\lambda_1 = 286.3$ nm). Isotopic selectivity was achieved in the second excitation step at $\lambda_2 = 855.2$ nm by a narrowband continuous wave laser. Subsequently, resonant photoionization at $\lambda_3 = 694.7$ nm to a newly observed autoionizing state at 60,992.9 cm^{-1} provided efficient photoionization. The IS for all even and hyperfine splitting for odd isotopes have been measured for the 855.2 nm transition. A selectivity factor of 24 is achieved for ^{124}Sn isotope. The absorption cross sections of the three excitation steps is reasonably high to have an efficient photoionization scheme.

1 Introduction

Pure isotopes of an element have numerous applications in the fields of science, medicine, and industry. Among the various isotope enrichment methods, the one using lasers is considered to be efficient and economical. Recent years have seen the building of facilities for isotope separation based on atomic vapor laser isotope separation (AVLIS) technique [1, 2]. Tin has ten naturally occurring isotopes, and some of them are known to be useful for nuclear, medical, and scientific applications. It is worthwhile to mention

here few specific applications of enriched tin isotopes. For instance, the ^{113}Sn is used in a ^{113}Sn–^{113m}In generator. The ^{113m}In is a low-energy γ emitter with a half-life of 1.16 h and is employed in biological, chemical, and physical studies [3, 4]. Enriched ^{112}Sn isotope is used for production of ^{113}Sn by (n, γ) reaction in the nuclear reactor. The ^{117m}Sn isotope is a potential therapeutic radionuclide for a treatment of the palliation of pain from bony metastases [5]. The ^{117m}Sn is produced in nuclear reactor using two nuclear reactions ^{116}Sn(n, γ)^{117m}Sn and ^{117}Sn(n, n′γ)^{117m}Sn where enriched ^{116}Sn and ^{117}Sn targets are used, respectively [6]. The investigation of properties of neutrinos is one of the most important problems in fundamental physics. Neutrino flavor-oscillation experiments have established that neutrinos have non-zero mass [7, 8]. The study of neutrinoless double beta decay (0νββ) is important for investigation of the mass and nature of the neutrino, which is of fundamental importance [9]. The India-based TIN detector (*TIN.TIN*) is proposed for the search of 0νββ decay in ^{124}Sn at the upcoming underground India-based Neutrino Observatory (INO) [10]. Among the 0νββ decay candidates in the tin isotopes, the ^{124}Sn isotope (with natural abundance of is 5.79%) is chosen due to its

✉ S. G. Nakhate
nakhate@barc.gov.in

1 Atomic and Molecular Physics Division, Bhabha Atomic Research Centre, Mumbai 400085, India

2 Laser and Plasma Technology Division, Bhabha Atomic Research Centre, Mumbai 400085, India

3 Homi Bhabha National Institute, Anushaktinagar, Mumbai 400094, India

4 Tata Institute of Fundamental Research, Mumbai 400005, India

reasonably high Q value of 2.28 MeV. The highly enriched isotopes of tin are commercially produced presently by centrifuge method [11]. However, laser isotope separation (LIS) is an efficient and suitable method, especially for radioactive isotopes and isomers. The primary motivation behind the present work is to investigate the isotope-selective stepwise resonance ionization scheme for enrichment of the [124]Sn isotope, which is required for the proposed *TIN. TIN* detector [12].

The tin atom has three fine-structure ground state levels $5s^2 5p^2$, $^3P_{0-2}$, and absorption lines arising from these levels lie in the UV region. Moreover, tin being in the middle of the periodic table, the isotopes suffer from the small isotope shifts (IS), which is unfavorable for laser isotope separation. An added disadvantage is the short radiative lifetimes of the excited levels of a few-to-tens of nanoseconds. A few resonance ionization schemes (RIS) were investigated in the past [13, 14] for efficient laser ion source or trace detection. The review of RIS schemes with atomic parameters is given by Soloman [15]. An anomalous odd- to even-mass isotope ratio in resonance ionization with broadband lasers was also reported by Fairbank et al. [16]. None of the RIS schemes investigated in the past are isotope-selective. The first excitation step for tin RIS is in UV and requires frequency-doubled tunable laser. The IS in tin are known for only two lines, 286.3 [17, 18] and 326.2 nm [19], and are in the range of 180–320 MHz between the consecutive pairs of even isotopes. In the present paper, we propose a three-color, three-photon RIS scheme which requires broadband pulsed laser excitation at 286.3 nm and then isotope-selective excitation at the second step in red at 855.2 nm by a narrowband continuous wave (cw) laser and the third step to the newly observed autoionizing state with substantially large ionization cross section by a pulsed laser. This avoids the need for a narrowband frequency-doubled UV laser with low pulse–pulse temporal jitter of ~ 1 ns. We measured IS for all even isotopes and hyperfine splitting (HFS) for the abundant odd isotopes for the proposed isotope-selective 855.2 nm transition. We also determined the isotope selectivity factor, α, for all naturally occurring isotopes, except [115]Sn, which has a natural abundance of only 0.34%.

2 Experimental

Laser vaporization of a tin rod followed by supersonic expansion in a molecular beam apparatus provided the atomic beam of tin [20]. The first chamber contains the pulsed nozzle, a Smalley-type ablation source with rotating and translating tin rod. Laser vaporization was carried out by a Q-switched Nd:YAG laser (Quanta System, SYL 203), at 355 nm, pulse energy ~ 5 mJ focused to a spot size of ~ 0.5 mm diameter. The atomic beam is skimmed at a

distance of 200 mm from the nozzle into a second chamber which houses a linear time-of-flight mass spectrometer (TOFMS), mounted orthogonal to the atomic beam axis. The distance between the nozzle and the photoionization spot in the TOF is 620 mm. Tin atoms were resonantly excited to the first step at $\lambda_1 = 286.3$ nm by a 6 GHz linewidth frequency-doubled pulsed dye laser having ~ 10 ns pulse duration (Coherent, ScanMatePro) pumped by a XeCl excimer laser (Coherent, CompexPro 201). Atoms were excited to the second step by a narrowband (< 1 MHz) cw diode laser (TUI Optics, DL100). The crossed laser beams intersect the atomic beam and are mutually orthogonal. A third laser beam, either from a Q-switched Nd:YAG laser (Litron Lasers, Nano SG 120) at 532 nm or another tunable pulsed dye laser (Lamda Physik, FL3002) pumped by the same excimer laser, respectively, provided either a non-resonant ionization or excitation to an autoionizing state. Pulse duration of Nd:YAG laser was ~ 6 ns. The third laser was passed collinearly along the cw laser by combining with a dichroic mirror or polarizing beam combiner. The laser beam diameter of ~ 3.7 mm was maintained by an iris on both sides of the entrance windows of the chamber. The shape of the intersection region of the lasers and atomic vapor is a cylinder of diameter 3.7 mm and length ~ 10 mm. The spatial overlap among the three laser beams was ensured in the interaction zone. Time delay of the third step laser viz. Nd:YAG or dye laser with respect to the first step laser was optimized for maximum photoionization signal either by electronic or optical delay, respectively. The digital delay generator (Stanford Research, DG535) was used for introducing appropriate delays between various synchronous events. Following ionization, ions were accelerated out of the ionization region, travelled 550 mm field-free drift tube of a TOFMS and were detected by a 25 mm diameter chevron-type microchannel plate detector (Burle). The detector output was amplified by a preamplifier (Femto Messtechnik, DUPVA-1) and recorded on a digital oscilloscope (Tektronix TDS 2024). The mass resolution of the TOFMS achieved in the present experiment is ~ 400.

To detect a three-color photoionization signal, pulse energy of the first step excitation dye laser was kept < 1 μJ; higher pulse energies led to non-resonant two-photon ionization to continuum by 286 nm photons. The power of the cw laser was 25 mW and the pulse energy of the ionization laser was kept at saturation energy. For measuring the isotope shift, λ_1 was fixed and λ_2 was scanned at a rate of 5 MHz/s. A box car averager (Stanford Research System, SR250) in static gate operation mode was used, and the time position of the sampling gate corresponding to the maxima of a target isotope in TOF spectrum was fixed. The IS for even isotopes was measured relative to [120]Sn by employing two channels of boxcar averager. The spectral linewidth of ~ 100 MHz was obtained in the experiment, which was limited by the

residual Doppler broadening in the supersonic beam. High-precision wavelength meter (High Finesse, WS7) provided absolute wavelength calibration for the cw laser with an accuracy of 30 MHz (3σ criteria).

3 Results and discussion

3.1 Isotope shift and hyperfine constants

The isotope-selective photoionization scheme used in the present work is following: $5s^2 5p^2, {}^3P_0 \xrightarrow{\lambda_1 = 286.331 \text{ nm}}$ $5s^2 5p6s, {}^3P_1 \xrightarrow{\lambda_2 = 855.253 \text{ nm}} 5s^2 5p6p, {}^1P_1 \xrightarrow{\lambda_3 = 532/694.75 \text{ nm}}$ non-resonant or autoionization.

The magnitude of IS and HFS is very important in multistep laser isotope separation. Tin lies in the middle of the periodic table, and isotope shifts are least in this region. The isotope shifts and HFS are known in the first step at 286.3 nm line [17, 18] and varies from 207 MHz in ^{124}Sn–^{122}Sn to 320 MHz in ^{112}Sn–^{114}Sn. The second step lies in the red wavelength region, and it is comparatively easy to operate a narrowband tunable laser in this wavelength region than in the frequency-doubled UV region.

Polarization of the excitation lasers plays a crucial role for selective excitation of odd–even isotopes [21]. The selection rules for dipole-allowed transitions for the π-polarized light are $\Delta J = 0, \pm 1$; $\Delta M_J = 0$ except for $\Delta J = 0$, and $M_J = 0 \leftrightarrow 0$. For odd isotopes, the selection rules for dipole-allowed transitions are $\Delta F = 0, \pm 1$; $\Delta M_F = 0$ except for $\Delta F = 0$, and $M_F = 0 \leftrightarrow 0$. Linearly polarized ($\pi$) light was used in the first step which excited population from the ground state ($J = 0$, $M_J = 0$) to the first excited state ($J = 1$, $M_J = 0$). In the second step, if a π-polarized light is used, excitation of even isotopes is forbidden by the dipole selection rules; however, odd isotopes are excited to the magnetic sublevels (M_F) of the 5p6p,${}^1P_1$ level. This effect was seen by substantial suppression of photoionization signal of even isotopes using π excitation in the first and second steps. However, use of circular polarized light (σ^+ or σ^-) in the second step allows excitation of both even and odd isotopes by dipole section rules ΔM_J, $\Delta M_F = \pm 1$.

The IS and HFS for the 855.2 nm transition are measured for the first time in this work and is shown for the ^{116}Sn and ^{119}Sn isotopes with respect to ^{120}Sn in Fig. 1. The J quantum number for both states in the 855 nm transition is 1, and major odd isotopes, ^{117}Sn and ^{119}Sn, have nuclear spin $I = 1/2$. Thus, four hyperfine components, F'–$F'' = 3/2$–$1/2$, $1/2$–$1/2$, $3/2$–$3/2$, and $1/2$–$3/2$, are expected for the odd isotopes and are shown in Fig. 1 for ^{119}Sn with the assignments. The observed intensity pattern of the hyperfine components is in agreement with the assignment. The energy of
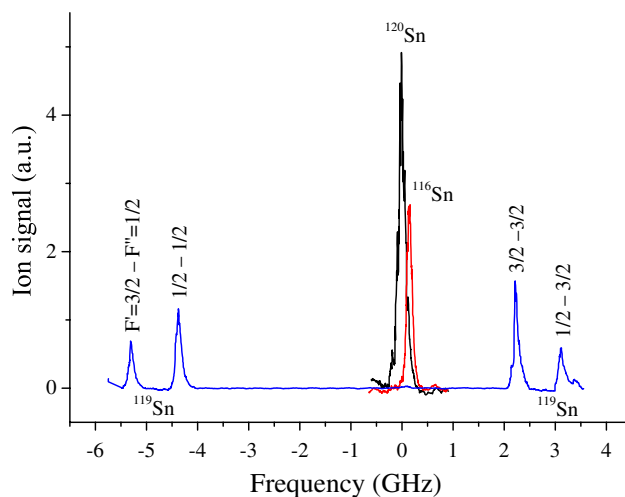

Fig. 1 Isotope shift and hyperfine structure spectra in ^{116,119}Sn recorded with reference to ^{120}Sn isotope in the 855.253 nm transition

Table 1 Isotope shifts (IS) for even isotopes of Sn I in 855.253 nm line

Isotopes	Isotope shift relative position (MHz)	Hyperfine constant, A (MHz)	Natural isotopic abundance (%)
112	0.0		0.97
114	−84		0.66
116	−169		14.54
117	−210	−553.7	7.68
118	−240		24.22
119	−270	−636.8	8.59
120	−309		32.58
122	−369		4.63
124	−405		5.73

Maximum error (1σ) in IS is 10 MHz

a hyperfine level for nucleus having spin $I = 1/2$ is given by Casimir formula [22].

$$W_F = W_J + \frac{A}{2}(J(J+1) - I(I+1) - F(F+1)), \qquad (1)$$

where A is hyperfine constant, and W_J is center of gravity (CG) of the energy level having total angular momentum, J. The hyperfine constant, A in the lower state 5p6s,${}^3P_1$, in this transition were reported by earlier workers [17, 18]. The observed hyperfine transition frequencies in the present work and A values from ref [18]. were used to calculate the hyperfine constants and the center of gravity (CG) of the upper state 5p6p,${}^1P_1$, for ^{117}Sn and ^{119}Sn. The isotope shifts for even isotopes and center of gravity (CG) and hyperfine constant, A for odd isotopes are listed in Table 1. The maximum error of 10 MHz (1σ) was obtained by averaging of about

five traces. We could not detect HFS components of [115]Sn due to its low natural abundance; however, the mass peak of [115]Sn appeared with 3/2–1/2 HFS component of [119]Sn, possibly due to overlap of one of its HFS components. IS for this transition is negative and is in accordance with the 5p6s → 5p6p transition.

The IS between the pair of isotopes A and A' in a spectral line i is given by [22]:

$$\delta v_{i;AA'} = F_i \langle \delta r^2 \rangle_{AA'} + M_i g_{AA'} \tag{2}$$

where F_i is proportional to the difference in the total probability density of the electrons at the nucleus in the two levels of the transition. For the 855 nm line, F_i is negative since the density in the upper level is less than the lower level. The $\langle \delta r^2 \rangle_{AA'}$ is the difference in the nuclear mean square charge radii between isotopes A and A'. M_i is the mass shift between the isotopes [118]Sn and [116]Sn, and $g_{AA'} = \frac{m_A - m_{A'}}{m_A \cdot m_{A'}} \frac{m_{118} \cdot m_{116}}{m_{118} - m_{116}}$, where m_A and $m_{A'}$ are nuclear masses. Self-consistency of the IS measurements in the 855 nm transition can be checked from the King plot [22] (Fig. 2) between the 855 and 286 nm lines. The IS data for the 286 nm line were taken from earlier measurements [17, 18]. All the IS in 855 and 286 nm lines are scaled by a factor $g_{AA'}$, that is $\delta v_{1AA'}/g_{AA'}$ and $\delta v_{2AA'}/g_{AA'}$, respectively. When plotted against each other, should give a straight line according to Eq. (2) with slope $\phi = F_1/F_2$ and intercept $\mu = M_1 - \phi M_2$. Figure 2 shows the consistency of the results for the two lines is fair. This could be attributed to the relatively large measurement error of ± 10 MHz in the IS values ranging from 85 to 35 MHz in the 855 nm line between the successive pairs of isotopes. We find $\phi = -0.38$ (2) and $\mu = 39$ (7) MHz. From these values, we derived $F_1 = -1245$ (200) MHz fm^{-2} and $M_1 = 76$ (28) MHz
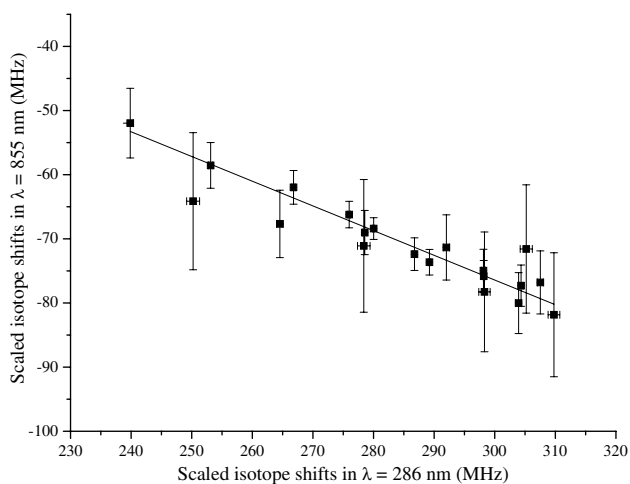
for the 855 nm line, where we used $F_2 = 3.3$ (5) GHz fm^{-2} and $M_2 = -98$ (70) MHz for the 286 nm line [17]. The uncertainties in F_1 and M_1 values are large due to large errors in F_2 and M_2.

3.2 Isotope selectivity

The IS of [124]Sn from the abundant isotopes [120]Sn and [118]Sn is, respectively, 96 and 165 MHz. However, the $\Delta \nu(124–122)$ is only 36 MHz, which is small compared to the Doppler-broadened linewidth of ~100 MHz achieved in this experiment. Figure 3 shows a series of TOF mass spectra following stepwise isotope-selective photoionization achieved with the cw diode laser in the second step tuned to the even isotopes.

The traces show that selective ionization of all even isotopes is feasible including the isotope of interest [124]Sn. The isotope selectivity α for a particular isotope, for example [124]Sn is defined as:

$$\alpha^{124} = \frac{\left[{}^{124}I \middle/ \left(\sum I - {}^{124}I \right) \right]_\lambda}{\left[{}^{124}f \middle/ \left(1 - {}^{124}f \right) \right]_{\text{natural}}}, \tag{3}$$

Fig. 2 King plot of isotope shifts measured in present work in 855.2 nm line verses 286.3 nm line of Sn I. The solid squares show the scaled isotope shifts in various isotope pairs of Sn and the solid line is a linear fit to these points
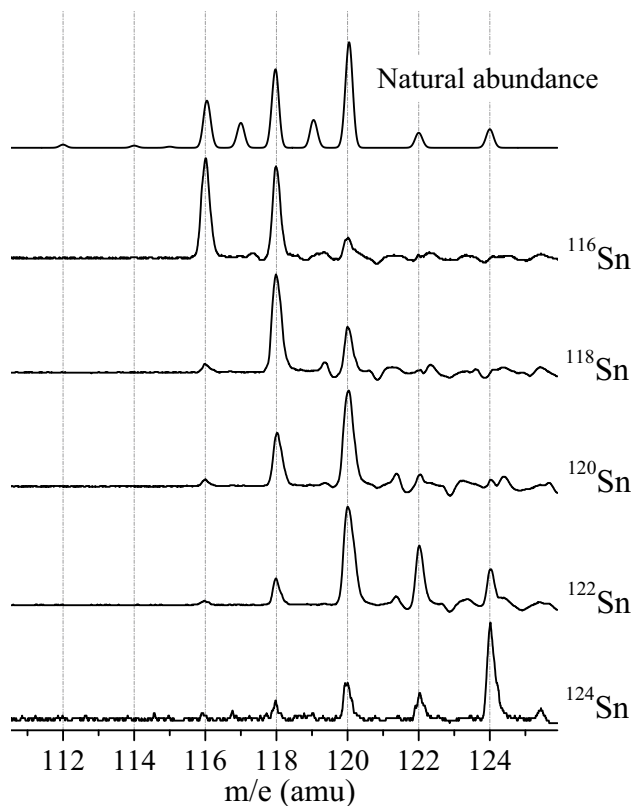

Fig. 3 A series of time-of-flight mass spectra following excitation with the narrowband cw diode laser wavelength, λ_2 tuned to the maxima of the indicated tin isotope. The top trace depicts natural abundance of the tin

Table 2 Selectivity factor, α for Sn isotopes at their excitation peak wavenumber, λ_2

Sn isotope	Selectivity factor, α	Excitation wavenumber (second step)
124	24	11,689.232
122	6	11,689.234
120	4	11,689.236
118	7	11,689.238
116	6	11,689.240
114	17	11,689.243
112	18	11,689.246
117	83	11,689.098
119	69	11,689.087

where ^{124}I and ΣI represent the ion signal intensities of ^{124}Sn and of all isotopes of Sn, respectively, at the excitation wavelength λ, and ^{124}f is the fractional natural abundance of ^{124}Sn. The selectivity factor, α achieved for ^{124}Sn isotope is 24. The selectivity factors for all tin isotopes are listed in Table 2 along with their excitation wavenumbers in the second step. Since the HFS components of ^{117}Sn and ^{119}Sn isotopes are separated by about 2–4 GHz from the bunch of even isotopes, the α for the odd isotopes are high compared to the even isotopes

3.3 Estimate of saturation energies and autoionizing resonances

In addition to isotope shifts and hyperfine structures, other parameters like radiative lifetime, transition probabilities, absorption cross sections and saturation energies are important for devising an efficient isotope-selective photoionization scheme. Radiative lifetime of the $5s^25p6s,^3P_1$ level involved in the 286.3 nm transition is 4.75 (18) ns [23] and transition probability is 5.4×10^7 s^{-1} [24]. The estimated laser pulse energy [15] required to saturate this strong UV transition is very small, ~ 0.4 μJ/cm^2, and thus was employed in this experiment. We have measured the radiative lifetime for the second excited level, $5s^25p6p,^1P_1$ by changing the time delay between the $\lambda_1 = 286.3$ nm and ionization laser $\lambda_3 = 532$ nm using digital delay generator. The second step excitation at $\lambda_2 = 855.2$ nm is continuous. Figure 4 shows the plot of photoionization signal intensity of ^{120}Sn versus time delay between the λ_1 and λ_3 excitation laser pulses. Least squares fit to the data results in a radiative lifetime of 33 (1) ns for the $5s^25p6p,^1P_1$ level. The branching fraction for the 855.2 nm transition is estimated as 0.377 from the available relative intensity data of the emission lines originating from $5s^25p6p,^1P_1$ [24]. The transition probability, calculated from the radiative lifetime and branching fraction is 1.1×10^7 s^{-1}, is also
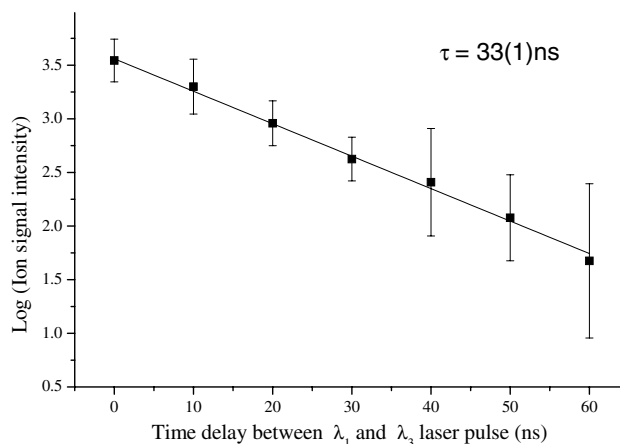
Fig. 4 Population decay of the $5s^25p6p,^1P_1$ excited level of Sn I at 46,603.517 cm^{-1}. The solid line is a linear fit to the data points

substantial. In the present experiment, the second excitation step at 855.2 nm was carried out by a single mode cw laser of ~ 1 MHz linewidth; however, the Doppler width of the Sn atomic beam is ~ 100 MHz. Thus, even by employing cw laser power more than saturation intensity of ~ 105 mW cm^{-2} (estimated from the transition probability and Doppler width), the available Sn atoms population in the $5s^25p6s,^3P_1$ level by 1 MHz band cw laser is not addressed. The laser linewidth should be similar to the Doppler width of the atom for optimum excitation. Alternatively, it can be realized by generating a frequency comb with a controllable envelope by modulating the injection current of the diode laser.

The third step is photoionization and was carried out either by non-resonant photoionization to the continuum by 532 nm pulsed laser or by autoionization in the wavelength range $\lambda_3 = 670$–750 nm. Six autoionizing (AI) resonances accessible from the $5s^25p6p,^1P_1$ level are listed in NIST data table [24] at energies 60,397.1, 60,646.1, 60,946, 60,968, 61,215.2, and 61,365 cm^{-1}. Other than the AI state at 60,946 cm^{-1}, we observed other AI resonances as broad and weak. In addition to these listed resonances [24] we observed very strong and relatively sharp new AI resonance at 60,992.9 cm^{-1}. The ionization cross section for this new AI resonance was determined by measuring ionization yield of ^{120}Sn isotope as a function of laser energy in the third step and is shown in Fig. 5. The saturation laser energy flux, ε_{sat} is calculated by fitting the experimental data points to the expression [15].

$$I = I_0 \left(1 - e^{\left(\frac{\varepsilon}{\varepsilon_{sat}} \right)} \right), \tag{4}$$

where I is the ionization signal at laser energy flux ε, I_0 is the maximum ionization signal. A saturation energy flux
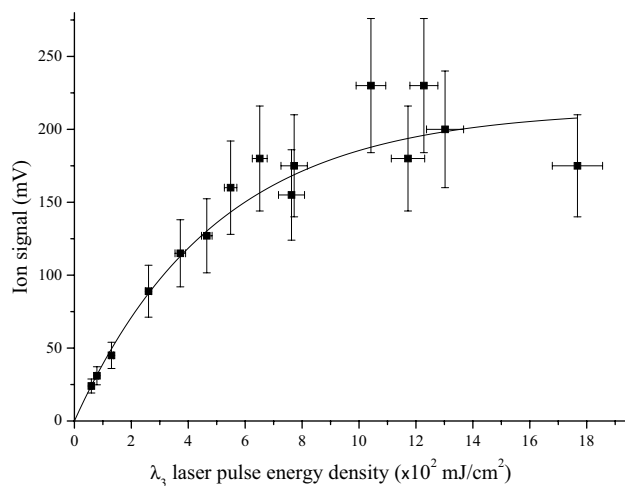
Fig. 5 Photoionization yield of ^{120}Sn isotope as a function of laser energy density in the third step (λ_3) leading to the autoionizing state at 60,992.9 cm^{-1} excited by $\lambda_3 = 694.75$ nm. The solid line is a fit to the experimental data to Eq. (4)

$\varepsilon_{sat} = 49.5$ μJ cm^{-2} was obtained. According to Soloman [15], this value can be transformed to $\sigma = \frac{10^{-18}}{5.03 \times 10^{-6} \times \lambda(nm) \times \varepsilon_{sat}(mJ\ cm^{-2})}$, yielding a cross section $\sigma_3 = 5.8\ (6) \times 10^{-15}$ cm^2. This cross section is two orders of magnitude greater than that of the non-resonant photoionization cross section of $5.4\ (9) \times 10^{-17}$ cm^2, determined at 532 nm.

4 Conclusion

The laser isotope separation scheme for tin isotopes has been demonstrated with a three-step, three-color laser photoionization scheme. A broadband (~ 4–6 GHz) pulsed dye laser was used to excite all Sn isotopes to the 5p6s excited state ($\lambda_1 = 286.3$ nm) from the 5p^2, ^{3}P$_0$ ground state, and then a narrowband tunable cw diode laser was used for isotope-selective excitation in the second step 5p6p, ^{1}P$_1$ ($\lambda_2 = 855.2$ nm). The third photon ($\lambda_2 = 694.7$ nm) efficiently photoionized the isotope-selected Sn atoms via newly observed autoionizing state with substantially large cross section. The hyperfine constant, A of the 5p6p excited states in ^{117}Sn and ^{119}Sn as well as the 6s–6p transition isotope shifts for all even Sn isotopes have been measured. The hyperfine components are well separated from the even isotopes. While the isotope shifts of $\Delta\nu(124–120) \sim 100$ MHz in the 855.2 nm excitation is a downside compared to the 440 MHz shifts in the 286.3 nm excitation; higher lifetime of 33 ns of the 5p6p state compared to 5 ns of the 5p6s state and the excitation wavelength being in red suggest a possible laser isotope separation scheme. The photoionization cross sections for the all three excitation steps are substantially large to achieve efficient photoionization at reasonable laser power.

References

1. A.B. D'yachkov, S.K. Kovalevich, A.V. Labozin, V.P. Labozin, S.M. Mironov, V.Ya. Panchenko, V.A. Firsov, G.O. Tsvetkov, G.G. Shatalova, Quantum Electron. **42**, 953 (2012)
2. H. Park, D.-H. Kwon, Y.H. Cha, T.-S. Kim, J. Han, K.-H. Ko, D.-Y. Jeong, C.-J. Kim, J. Nucl. Sci. Technol. **6**, 111 (2008)
3. M.H. Adatepe, M. Welch, R.G. Evens, E.J. Potchen, Am. J. Roentgenol. **112**, 701 (1971)
4. S. Wenhao, S. Daohai, H. Yong: In, Isotope production and applications in the 21st century, in P*roceedings of the 3rd International conference on Isotopes*, vol 226, ed. by N.R. Stevenson (World Scientific Publishing Co. Pte. Ltd., London, 2000)
5. S.C. Srivastava, H.L. Atkins, G.T. Krishnamurthy, I. Zanzi, E.B. Silberstein, G. Meinken, L.F. Mausner, F. Swailem, T. D'Alessandro, C.J. Cabahug, Y. Lau, T. Park, S. Madajewicz, Clin. Cancer Res. **4**, 61 (1998)
6. S.C. Srivastava, in *Technetium, Rhenium and Other Metals in Chemistry and Nuclear Medicine*, ed. by M. Nicolini, E. Mazzi (SGE Editoriali, Padua, 1999), p. 305
7. Y. Fukuda, Super-Kamiokande Collaboration et al., Phys. Rev. Lett. **81**, 1562 (1998)
8. R. Wendell, Super-Kamiokande Collaboration et al., Phys. Rev. D **81**, 092004 (2010)
9. O. Cremonesi, M. Pavan, Adv. High Energy Phys. **2014**, 951432 (2014)
10. N.K. Mondal, Pramana **79**, 1003 (2012)
11. V.Y. Baranov, in *Isotopes: Properties, Preparation, Applications* (Izdat; Moscow, 2000), p. 703 (**ISBN 5-86656-100-X**)
12. V. Nanal, EPJ Web Conf. **66**, 08005 (2014)
13. J.C. Travis, J.D. Fassett, L.J. Moore: In, *Resonance Ionization Spectroscopy: A Survey of Elements Detected Using Resonance Ionization Mass Spectrometry with Thermal Vaporization*, ed. by G.S. Hurst, M.G. Payne (The Institute of Physics, Bristol 1984), p. 97
14. F. Scheerer, F. Albus, F. Ames, H.-J. Kluge, N. Trautmann, Spectrochim. Acta B **47**, 795 (1992)
15. E.B. Saloman, Spectrochim. Acta B **47**, 517 (1992)
16. W.M. Fairbank Jr, M.T. Spaar, J.E. Parks, J.M.R. Hutchinson, Phys. Rev. A **40**, 2195 (1989)
17. P.E.G. Baird, S.A. Blundell, G. Burrows, C.J. Foot, D.N. G.Meiselt, G.K. Stacey, Woodgate, J. Phys. B At. Mol. Phys. **16**, 2485 (1983)
18. M. Anselment, K. Bekk, A. Hanser, H. Hoeffgen, G. Meisel, S. Goring, H. Rebel, G. Schatz, Phys. Rev. C **34**, 1052 (1986)
19. J.D. Silver, D.N. Stacey, Proc. R. Soc. Lond. A **332**, 129 (1973)
20. S. Mukund, S. Bhattacharyya, S.G. Nakhate, J. Quant. Spectr. Rad. Trans. **147**, 274 (2014)
21. L.C. Balling, J.J. Wright, Appl. Phys. Lett. **29**, 411 (1976)
22. H.G. Kuhn, in *Atomic Spectra* (Longmans, London, 1969)
23. L. Holmgren, S. Svanberg, Phys. Ser. **5**, 135 (1972)
24. A. Kramida, Yu Ralchenko, J. Reader, NIST ASD Team, NIST Atomic Spectra Database (ver. 5.6.1), [Online] National Institute of Standards and Technology, Gaithersburg, MD. https://physics.nist.gov/asd. Accessed 29 Nov 2018. (2018). https://doi.org/10.18434/T4W30F